Insights from modeling metabolism and amoeboid cell motility in the immune system

Steijn, L. van

Chapter 3

Cell-matrix adhesion affects cell motility mode: from short-term persistent to long-term subdiffusive modes

Leonie van Steijn, Clément Sire, Loïc Dupré, Guy Theraulaz, Roeland M.H. Merks*

Abstract

Lymphocytes have been described to perform different motility patterns such as Brownian random walks, persistent random walks, and Lévy walks. Depending on the conditions, such as confinement or the distribution of target cells, either Brownian or Lévy walks lead to more efficient interaction with the targets.The diversity of these motility patterns may be explained by an adaptive response to the surrounding extracellular matrix (ECM). Indeed, depending on the ECM composition, lymphocytes either display a floating motion without attaching to the ECM, or sliding and stepping motion with respectively continuous or discontinuous attachment to the ECM, or pivoting behaviour with sustained attachment to the ECM. Moreover, on the long term, lymphocytes either perform a persistent random walk or a Brownian-like movement depending on the ECM composition. How the ECM affects cell motility is still incompletely understood. Here, we integrate essential mechanistic details of the lymphocyte-matrix adhesions and lymphocyte intrinsic cytoskeletal induced cell propulsion into a Cellular Potts model (CPM). We show that the combination of *de novo* cell-matrix adhesion formation, adhesion growth and shrinkage, adhesion rupture, and feedback of adhesions onto cell propulsion recapitulates multiple lymphocyte behaviours, for different lymphocyte subsets and various substrates. With increasing attachment area and increased adhesion strength, the cells' velocity and persistence decreases. Additionally, the model can predict short-term persistent with long-term subdiffusive

*Submitted as Leonie van Steijn et al. "Computational modelling of cell motility modes emerging from cell-matrix adhesion dynamics", available on bioRxiv, https://doi.org/10.1101/2021.06.09.447692

motility, showing a pivoting motion. For small adhesion areas, we observe that the spatial distribution of adhesions influences cell motility. Small adhesions at the front allow for more persistent motion than larger clusters at the back, despite a similar total adhesion area. In conclusion, we present an integrated framework to simulate the effects of ECM proteins on cell-matrix adhesion dynamics. The model reveals a sufficient set of principles explaining the plasticity of lymphocyte motility.

Author summary

During immunosurveillance, lymphocytes patrol through tissues to interact with cancer cells, other immune cells, and pathogens. The efficiency of this process depends on the kinds of trajectories taken, ranging from simple Brownian walks to Lévy walks. The composition of the extracellular matrix (ECM), a network of macromolecules, affects the formation of cell-matrix adhesions, thus strongly influencing the way lymphocytes move. Here, we present a model of lymphocyte motility driven by adhesions that grow, shrink and rupture in response to the ECM and cellular forces. Compared to other models, our model is computationally light making it suitable for generating long term cell track data, while still capturing actin dynamics and adhesion turnover. Our model suggests that cell motility is affected by the force required to break adhesions and the rate at which new adhesions form. Adhesions can promote cell protrusion by inhibiting retrograde actin flow. After introducing this effect into the model, we found that it reduces the cellular diffusivity and that it promotes stick-slip behaviour. Furthermore, location and size of adhesion clusters determined cell persistence. Overall, our model explains the plasticity of lymphocyte behaviour in response to the ECM.

3.1 Introduction

Lymphocytes patrol in tissues and are recruited to infected areas to detect and clear the area of pathogens and cancer cells. The type of walk by which lymphocytes patrol determines the efficiency of finding their target depending on the environment [137, 138, 139, 56, 140]. In the absence of obstacles, Lévy walks and persistent random walks outperform Brownian walks. Lévy walks are characterized by long strides in their trajectories such that they cover larger areas than Brownian walks. In environments crowded with obstacles Brownian walks perform better, as the more compact trajectory leads to more thorough local exploration [137]. Even more

local exploration follows from subdiffusive random walkers, which diffuse less far than could be expected from their speed and persistence. Consistent with these characteristics, in the densely populated lymph nodes T lymphocytes perform Brownian walks [53, 54] or persistent random walks [55]. In the brain tissue, T cells perform Lévy walks [56]. In pancreatic islets CD4+ T cells perform subdiffusive random walks, whereas CD8+ T cells perform confined random walks [57]. The characteristics of these different types of motion, including speed distribution and mean squared displacement (MSD), determine how efficiently lymphocytes can find their targets *in vivo*. Therefore it is key to understand what factors give rise to these different types of walks.

The plasticity of lymphocyte motility behaviour is dictated both by environmental factors and by cell intrinsic features [141, 142]. An *in vitro* study has shown that the type of extracellular matrix (ECM) used as cell culture substrate affects the motility patterns of B lymphocytes, possibly due to the attachment strength [143]. On fibronectin, B lymphocytes show higher diffusivity and more effective displacement than on collagen IV substrates where cells move more slowly. The B lymphocytes formed larger adhesive connections with fibronectin than with collagen IV, and on fibronectin the cells changed shape more rapidly than on collagen IV. Similar effects have been found for T lymphocytes. The majority of cells on a casein substrate move through multiple, distinct and temporary adhesion zones, i.e., walking motility, whereas on ICAM-1 substrates, the majority of cells make one continuous contact zone with the substrate, i.e., sliding motility [144].

Cells also show large individual variation in their motility patterns. On fibronectin, individual B lymphocytes showed either floating-like behaviour with little attachment, dynamic attachment leading to stepping/walking behaviour, or sustained attachment leading to cells pivoting around their adhesive area [143]. Similarly, T lymphocytes showed either walking, mixed or sliding behavior, with frequencies depending the type of culture substrate [144].

It is still poorly understood what causes, on the one hand, the consistent differences in motility modes between culture substrates, and on the other hand, the large individual differences between cells on the same type of substrate. To answer this question, here we propose a simplified mathematical model of cell motility and the adhesive interaction with the ECM.

Previous modeling studies have already provided useful insight into this problem. Copos et al. [145] asked what causes the cellular extension and retraction cycles driving the motility of *Dictyostelium discoideum* cells.

They modelled *D. discoideum* movement in a force-based model. Depending on the density of adhesion binding sites in the substrate, or the strength of these adhesions, the model displayed different motility types. For low densities of adhesion binding sites in the substrate and low adhesion strength, gliding motility was observed. Increasing the density of the binding sites or the adhesion strength led to a stepping motility mode of reduced speed. For the highest adhesion densities or adhesion strengths the cells became stationary. Thus the cells moved faster in the gliding motility mode than in the stepping motility mode. Although this agreed with preliminary experimental results on *D. discoideum* cells[145], these results contradict observation in lymphocyes: T cells move faster in stepping motility mode than in gliding motility mode [144]. Furthermore, as a one-dimensional model, it cannot produce two-dimensional cell tracks and it is computationally too heavy for producing the large amounts of cell track data required for our purpose.

Phase field models make it possible to study the effect of ECM on cell motility in two dimensions [65, 67]. In [65], the model includes actin polymerization, explicit dynamics of adhesion site formation and substrate compliance. Simulated cells displayed a gliding motion when substrate stiffness was high, the protrusion strength was large and adhesions formed at a high rate. At intermediate substrate stiffnesses with sufficiently high protrusion strength and intermediate adhesion formation, the cells displayed a stick-and-slip motion. Yet, the computational costs are still too high for the length and number of cell track data we require for statistical analysis.

Yu et al. [146] introduced a computationally efficient, coarse-grained model to study long term cell persistence. The model considered spheroid cells with a fixed pool of focal adhesions. These adhesions were assumed to be widely dispersed within the cells for soft substrates and more narrowly dispersed for rigid substrates. The increased persistence times on rigid substrates led to durotaxis, i.e. preferential movement towards stiffer substrates. However, Yu et al. imposed a direct dependence of cell persistence on adhesion distribution. In our work, we hope to explain this relation emerging from first principles.

Thus, previous models are either too computationally expensive or do not model the effect of adhesion on the microscopic level. The Cellular Potts model is conceptually closely related to phase fields model, but is computationally much lighter. The Act model [73], a recent extension of the Cellular Potts model, provides of phenomenological model of actin dynamics. Interestingly, this model can already display multiple motility

modes: Simulated cells show intermittent (stop-and-go) or persistent random walks. An in-depth characterization revealed that the model displays universal coupling between speed and persistence, and specifically that speed increases linearly with protrusion strength, whereas persistence time increase exponentially with protrusion strength [147].

Here we extend the Act model with cell-ECM interactions. The model combines coarsed-grained actin dynamics, with simplified dynamics of adhesion turn-over and detachment, resulting in a diverse palette of cell motility. In a second version of the model, the cell-ECM adhesions promote cell protrusion by inhibiting retrograde actin flow. Our model can simulate cell motion with sufficient detail on the location and size of adhesive patches, while being computationally light enough for statistical analysis of cell motility. With the actin component and cell-matrix adhesion component of the model, we are able to reproduce a variety of cell motion types, similar to the behaviour seen in other models that also include those two components [145, 65, 67]. In addition to persistent random walks and ballistic cell motility, the extended model can also predict anomalous diffusion with long-term subdiffusive behaviour, showing all three phases of lymphocyte motility on fibronectin found in the experimental work by Rey-Barroso et al.[143]. Our model shows that simple cell-ECM interactions can drastically alter cell motility. Thus, adhesion dynamics can play a key role in the plasticity of motility in response to ECM composition.

3.2 Results

In this section, we present how we model the dynamics of cell-matrix adhesions. We show that this model can reproduce a wide range of lymphocyte motility modes. Next, we extend the model with feedback from the adhesions onto the actin polymerization force and show that we can capture more dynamic motility behaviours. Overall, our model recapitulates the diversity of lymphocyte motility modes and provides insight into the mechanisms underlying such behavioural diversity.

3.2.1 Modelling cell-matrix adhesions

Our computational model is based on the Act model [73], an extension of the Cellular Potts model (CPM, [148, 149]) with an actin-inspired feedback mechanism that results in realistic cell shapes and cell polarization. In short, this extension keeps track of recent “actin activity" through Act values at a subcellular level, and cell protrusion at sites with locally high Act values is favoured. Two important parameters for this are λ_{Act}, the weight of the Act

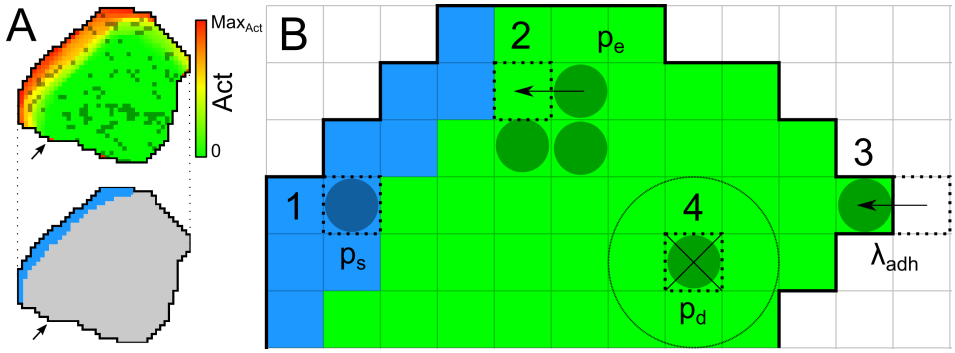

FIGURE 3.1: **Overview of the adhesion processes within the model.** A) Top: overview of a simulated cell. Red to yellow shading indicates the Act-level of each grid point. Darker coloured grid points contain an adhesion. Bottom: same cell with the region where new adhesions can form as the local Act-levels exceeds the $0.75\,\mathrm{Max}_{Act}$ threshold depicted in blue. Both: Arrows point to area with one grid point with high Act-level due to a recent extension of the cell (top, red), but the geometric mean of Act-levels does not exceed the threshold and hence new adhesions cannot form there (bottom, grey). B) Visual summary of adhesion processes. Dark coloured circles indicate grid points containing an adhesion. 1) New adhesions can form spontaneously with probability p_s at cell grid points where the geometric means of Act values exceeds the threshold of $0.75\,\mathrm{Max}_{Act}$ (blue region). 2) An adhesion patch can grow by Eden growth. A random neighbour of an adhesion site is selected. When it does not contain an adhesion yet, the patch extends into that grid point with probability p_e. 3) Adhesions can disbond spontaneously, depending on the number of neighbouring grid points without adhesions and probability p_d. 4) When cell retraction would break an adhesion, this is paired with a energy cost λ_{adh}.

model that can be interpreted as the maximum protrusive force of the actin network, and Max_{Act}, the maximum Act value, interpretable as the lifetime of an actin subunit within the actin network (see Table 3.1). In addition, our model takes cell-matrix adhesion into account and reflects the dynamic processes of such adhesions (Fig 3.1). We will shortly explain the addition of cell-matrix adhesions below. For further details, see the Method section.

Modelled cell-matrix adhesions are monitored at a subcellular level. A subcellular CPM grid point can either contain an adhesion or not. A single grid point is approximately 600 nm wide, considering that simulated cells contain approximately 1000 CPM grid points each, and that B cells and T cells on a substrate cover an area of approximately 360 μm^2[143, 150]. Observations show that single adhesion units in lymphocytes are

approximately 100 nm in diameter [150], so a single adhesion grid point in the model represents a small number (≤ 5) of adhesion units, considering adhesion unit density of 5 clusters/μm^2 [150].

The formation of new adhesions depends on actin polymerization, membrane protrusion and the distribution of integrins at the leading edge of the cell [151, 152, 153]. As actin activity and the leading edge are marked in the Act model by grid points with high Act values, we let new adhesions appear at grid points with a locally high Act-level: i.e. when the geometric mean of Act-level $Act(y)$ of $NB_\sigma(x)$, the Moore neighbourhood of grid point x restricted to the same cell as point x, exceeds a threshold $\left(\prod_{y \in NB_\sigma(x)} Act(y)\right)^{\frac{1}{|NB_\sigma(x)|}} \geq 0.75\,\mathrm{Max}_{Act}$, grid point x receives an adhesion with probability p_s (Fig 3.1A and 3.1B, process 1).

Once an adhesion has formed, it can either expand into an adhesion patch, or disbond. Patch expansion happens due to some membrane properties: membrane fluctuations lessen with membrane-matrix adhesion and hence allow for more integrins to bind the matrix [154], and the curvature of the membrane favours aggregation of integrins [155, 156]. We choose to model the effects of these properties in a phenomenological way, guided by the observations of Jacobelli et al. [144]. They report radial expansion of adhesion patches with some bias in the direction of the cell front. The Eden-growth model [157] gives radially expanding spherical objects, so we decided to use an Eden-like growth process to model adhesion patch expansion. During the update of the adhesion layer of the model, whenever a grid point with adhesion is selected, we also randomly select a neighbour. If that neighbour does not contain an adhesion, it gains one with probability p_e (Fig 3.1B, process 2).

Cell-matrix adhesions are not everlasting and they can disbond spontaneously or by force. We model two distinct disbonding processes. First, we consider a general and spontaneous disbonding of adhesions. As adhesion molecules undergo continuous turnover and experience stress from myosin-II, adhesions are broken constantly. Hence, we associate a probability with this process. Again, following the observations from [144] that patches dissolve concentrically due to the involvement of myosin-II, we let the disbonding probability depend on the local neighbourhood of the adhesion. An adhesion grid point surrounded by other adhesion grid points is likely within the centre of a patch and, hence, less likely to spontaneously disbond, whereas a single adhesion grid point with no neighbouring adhesions is quite likely to disappear. The probability that an adhesion site disbonds is $p_d \cdot \left(\frac{|\{nb \in NB(x) | Adh(nb)=0\}|}{|\{nb \in NB(x)\}|}\right)^2$, where $NB(x)$ indicates the Moore neighbourhood of grid point x (Fig 3.1B, process 3).

The second process that disbonds adhesions is adhesion rupture through retraction of the cell. We model this rupture only at the edge of the cell, where contraction forces of the cell can break bonds. Integrin bonds are known to show catch-slip bond behaviour, meaning that initially the bond strengthens with increase of force, but will still break if enough force is applied. Here we neglect this specific behaviour and associate a single required energy cost of λ_{adh} with the rupture of adhesions at the retracting edge (Fig 3.1B, process 4).

All in all, our model extension for adhesions is quite simple and computationally light. All adhesion dynamics are governed by the four parameters p_s, p_e, p_d and λ_{adh}. An overview of all the relevant parameters is shown in Table 3.1.

3.2.2 Adhesions lead to crawling and pivoting motions

From the newly introduced parameters p_s,p_e,p_d and λ_{adh}, the two parameters p_s and λ_{ahd} are most directly associated with properties of the ECM. We can interpret p_s, the probability with which new adhesions arise at sites with high actin activity, as multiple biological processes. One process is the rate at which integrin molecules bind to their ligands in the extracellular matrix. Higher rates would translate into higher p_s. Another process is the availability of integrins to the cell front. Transportation towards the cell front, integrin production and breakdown can thus all influence p_s. For λ_{adh}, there are two complementing interpretations. As λ_{adh} is defined as the energy required to break an adhesion, it describes both the binding affinity between integrins and their ligands, as well as the number of integrins bound in a single adhesion complex. Since we are interested in how lymphocytes adapt their behaviour to the ECM, we first look at the influence of these two ECM-associated parameters.

The proposed model displays various motility types. Cells crawl when λ_{adh} is low to moderate (Fig 3.2A,3.2C, Supplementary Video S1). Cell persistence decreases as λ_{adh} increases (Fig 3.2B,3.2D, Supplementary Video S1). When both λ_{adh} and p_s are high, i.e., when adhesions easily form and require much energy to break, cells will remain stuck in place on the matrix. However, they can still make protrusions around them, resembling a pivoting motion (Fig 3.2D, Supplementary Video S1).

Comparing these four parameter settings (Fig 3.2), the cell area that is covered with adhesions is mainly regulated by the parameter p_s. The velocity of the cell is fluctuating a lot more than the cell adhesion area, but is mostly affected by the parameter λ_{adh}. These observations are in large agreement with the observations of Rey-Barroso et al. that B cells on

TABLE 3.1: List of parameters involved in adhesion dynamics and values used for simulations.

Parameter	Description	Values Figs. 2-4	Figs. 6,7	Fig. 8
λ_{Act}	Weight of the Act-extension, the maximum protrusive force induced by actin polymerization	240	120, 240	240
Max_{Act}	Maximum value of the Act-field, actin lifetime	120	120	120
-	Act-value threshold above which adhesion formation is possible	0.75	0.75	0.75
p_s	Probability of new adhesion formation	0.004-0.020	0.001-0.004	0.003, 0.001
p_e	Probability of neighbouring grid site to become adhesion site if not already so.	0.0055	0.0055	0.0015, 0.004
p_d	Scaling of probability of disbonding adhesion site	0.0064	0.008	0.0032
λ_{adh}	Energy required to rupture adhesion upon retraction of the cell	20-100	20-100	60
f	Prefactor for the adhesion feedback onto Act model	-	b-1	b-1
b	Base value of f in absence of adhesions	-	0.5	0.5
s	Adhesion area fraction saturation threshold above which $f = 1$	-	0.1	0.12

fibronectin with dynamic adhesion surfaces showed walking behaviour, and cells with large and sustained adhesion surfaces displaced very little as they were unable to relocate the adhesion area [143]. They are also in agreement with the observation of Jacobelli et al. that T cells displaying a gliding motion with higher adhesion area have lower speed compared to cells with a walking motion with lower adhesion area [144].

3.2.3 Adhesions slow down cell motion and diminish dispersal

The examples shown in Fig 3.2 and Supplementary Video S1 indicate that higher adhesion area is correlated with lower speed and lower cell diffusivity. To further look into this relationship, we averaged the cell velocity and adhesion area of 1000 independent runs for different combinations of p_s and λ_{Adh} (Fig 3.3A). Increasing the value of p_s increases the average adhesion area, while increasing the value of λ_{Adh} decreases cell velocity. Moreover, p_s and λ_{Adh} seem to have a synergistic effect. The drop in instantaneous cell speed (from highest to lowest in Fig 3.3A about 50% smaller) is modest compared to the drop in diffusion coefficient (Fig 3.3B, about 380% smaller). The diffusion coefficient drops rapidly with increasing λ_{Adh}.

Highly adhesive cells show subdiffusive behaviour

To investigate the drop of the diffusion coefficient, we analysed the mean squared displacement and fitted the values with a persistent random walker model [47, 158]:

$$MSD(t) = 4\frac{\nu_{th}^2}{\gamma_1^2}\left(\gamma_1 t - 1 + e^{-t\gamma_1}\right), \tag{3.1}$$

with ν_{th} the walker's velocity and γ_1 its persistence time. However, this description fails at the short time scale, at which the CPM is mainly driven by the random fluctuation in grid points. Hence, we extended Eq. 3.1 with translational diffusion [159]:

$$MSD(t) = 4\frac{\nu_{th}^2}{\gamma_1^2}\left(\gamma_1 t - 1 + e^{-t\gamma_1}\right) + D_T t \tag{3.2}$$

Eq. 3.2 gives good fits, except for the higher $\lambda_{adh} = 80, 100$. For lower λ_{adh}, we obtained the persistence time from fitting Eq. 3.2, (data not shown): The larger drop in dispersal rate compared to instantaneous cell speed can be explained by loss of persistence with higher adhesion energies and adhesive areas.

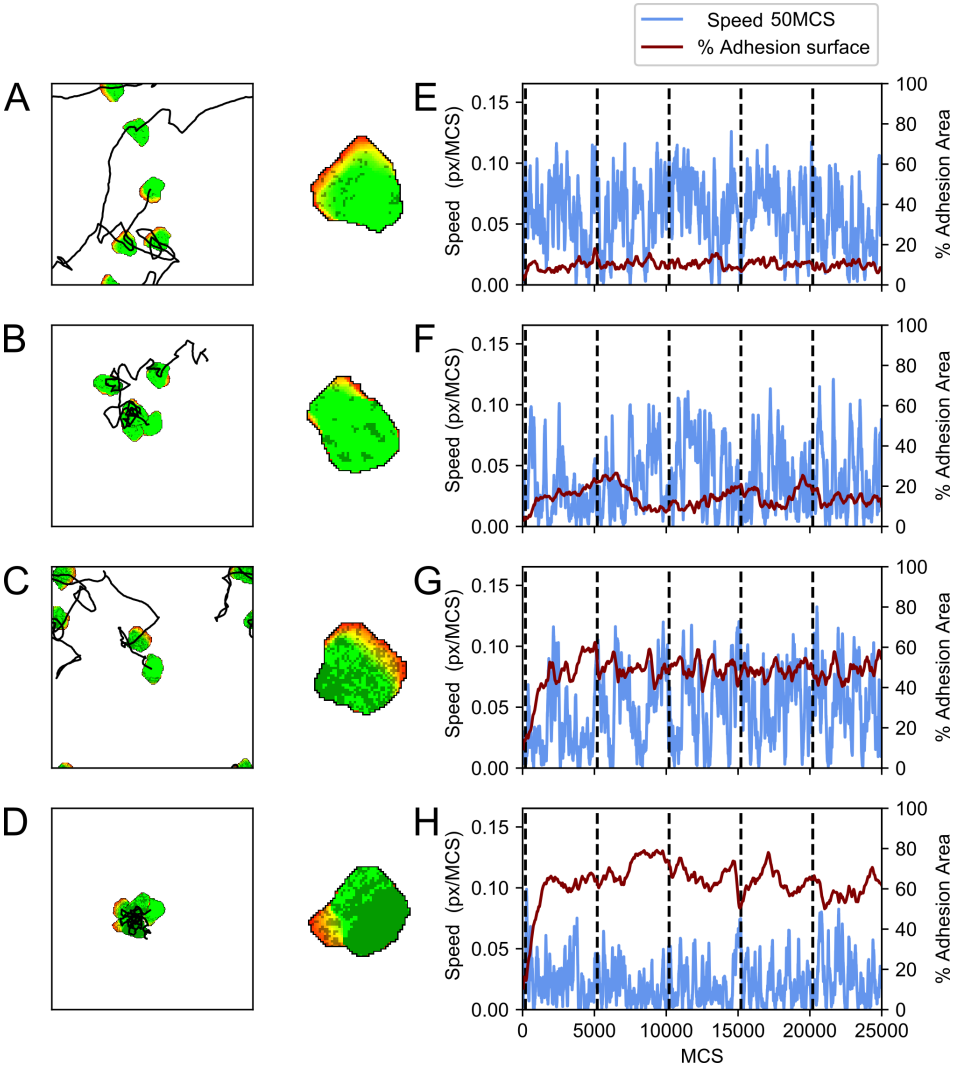

FIGURE 3.2: **Simulations of the model showing different motility types.** On the left, a display of a single cell at 5000 MCS interval snapshots combined with the cell centre's trajectory. Each trajectory starts in the centre of the field and periodic boundaries are used. In the middle, a close-up of the cell with the adhesions displayed in a darker colour. On the right, a plot of the cell's velocity and percentage of the cell's area containing adhesions corresponding to the track on the left. Vertical dashed lines indicate the times of the snapshots on the left. Parameters are: A) $\lambda_{adh} = 20$, $p_s = 0.004$, B) $\lambda_{adh} = 100$, $p_s = 0.004$, C) $\lambda_{adh} = 20$, $p_s = 0.02$, D) $\lambda_{adh} = 100$, $p_s = 0.02$. Furthermore, $p_d = 0.0008$ for A, B, C and D. These simulations are also available as Supplementary Video S1.

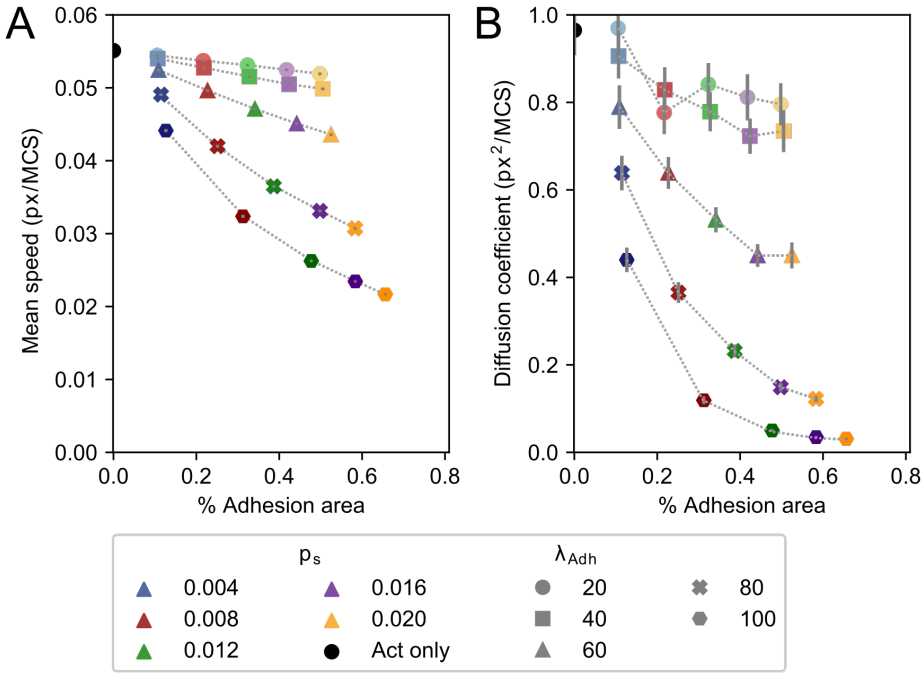

FIGURE 3.3: **Mean velocity, diffusion coefficient, and mean adhesive area change by increasing p_s and λ_{adh}.** Mean velocity (A) and diffusion coefficient (B) plotted against mean percentual adhesion area for different values of parameters p_s and λ_{adh}. Each dot represents the mean of 1000 independent simulations. Different colours indicate different p_s, where shades from light to dark and marker symbol indicate $\lambda_{Adh} \in \{20, 40, 60, 80, 100\}$. For reference, the mean velocity and diffusion coefficient of the Act model without any adhesions are indicated by a black circle. Error bars indicate 95% confidence intervals.

TABLE 3.2: Fitted values of α from Eq. 3.3 for different values of λ_{adh} and p_s

Parameters	α
$\lambda_{Adh} = 20, p_s = 0.004$	1.019
$\lambda_{Adh} = 20, p_s = 0.020$	1.013
$\lambda_{Adh} = 100, p_s = 0.004$	1.024
$\lambda_{Adh} = 100, p_s = 0.020$	1.257

For the parameter regime where Eq. 3.2 was a bad fit, we increased the initialization period left out of the MSD computation, in order to compute the MSD of cells closer to their dynamic equilibrium in both Act model dynamics as well as adhesion-extension dynamics. This barely improves the fit and suggests that cell motion in this regime cannot be correctly described by a persistent random walker with translational diffusion.

In [160] a fractional Klein-Kramers process was suggested as a good description of transformed Madin-Darby canine kidney cell motion. They fitted their data with

$$MSD(t) = 4v_{th}^2 t^2 E_{\alpha,3}(-\gamma_\alpha t^\alpha) + (2\eta)^2, \tag{3.3}$$

where $E_{\alpha,3}$ is the generalized Mittag-Leffler function and η is a noise term. The case where $\alpha = 1$ results in Eq. 3.1 except for the noise term. Since we already determined that translational diffusion plays significant role in the short-time scale of the CPM, we replaced the noise term with the term for translational diffusion, obtaining:

$$MSD(t) = 4v_{th}^2 t^2 E_{\alpha,3}(-\gamma_\alpha t^\alpha) + D_T t. \tag{3.4}$$

which reduces to Eq. 3.2 for $\alpha = 1$. This parameter α describes the long-term diffusive behaviour. For $t \to \infty$, Eq. 3.3, and by extension Eq. 3.4, can be approximated by $MSD(t) \sim \frac{4D_{th}t^{2-\alpha}}{\Gamma(3-\alpha)}$[160]. So for $\alpha > 1$, long-term behaviour is subdiffusive, whereas for $\alpha < 1$, long-term behaviour is superdiffusive.

In most cases where Eq. 3.2 fits well, we obtain $\alpha \approx 1$ (Table 3.2). However, for the cases were Eq. 3.2 fits badly, Eq. 3.4 has a better fit and $\alpha > 1$ (Fig. 3.4, Table 3.2). This corresponds to the cells stuck to the matrix and pivoting around their adhesion patch, as they are moving persistently on a local scale (a single protrusion front), but moving subdiffusively on a longer timescale.

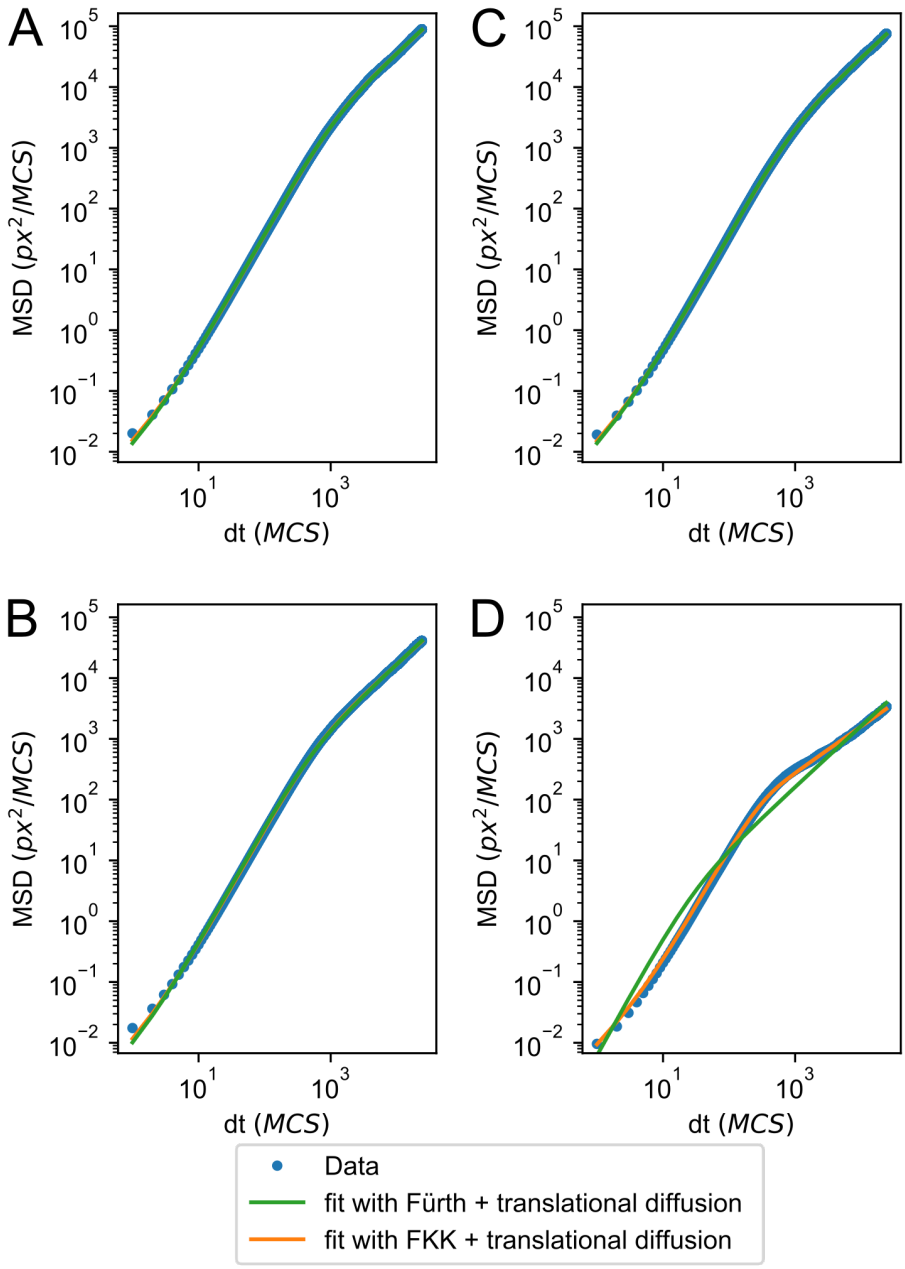

FIGURE 3.4: **MSD fits either a persistent random walker or a subdiffusive persistent random walker.** Log-log plot of MSD for the four scenarios in Fig. 3.2, with fits of Eqs. 3.2 and 3.4. Parameters are: A) $\lambda_{adh} = 20$, $p_s = 0.004$, B) $\lambda_{adh} = 100$, $p_s = 0.004$, C) $\lambda_{adh} = 20$, $p_s = 0.02$, D) $\lambda_{adh} = 100$, $p_s = 0.02$.

3.2.4 Modelling feedback of adhesions onto propulsion efficiency

This current model cannot explain the observation that B cells with a low adhesive area or no adhesive area on a fibronectin substrate show low displacement compared to cells with dynamic attachment [143]. Adhesions allow actin polymerization to lead to more efficient protrusions [161, 162, 163], as the force generated by the actin polymerization is transferred onto the matrix via the adhesion complex, instead of leading to treadmilling. When more of the actin network is connected to integrin complexes, a greater force resulting from actin polymerization can be transferred to the matrix. We mimic such behaviour using positive feedback between the adhesions and actin polymerization. We model this by defining a prefactor f which dynamically alters the weight of the Act-extension, and hence the propulsion force. For simplicity, we assume that protrusion efficiency will increase linearly with the cell's total adhesion area and will reach a point of saturation. Hence, we define:

$$f = \begin{cases} b + \frac{1-b}{s}\frac{A_{adh}(i)}{A(i)} & \text{if } \frac{A_{adh}(i)}{A(i)} \leq s \\ 1 & \text{if } \frac{A_{adh}(i)}{A(i)} > s \end{cases},$$

with b the baseline protrusion efficiency and s the saturation adhesion area. A schematic overview is shown in Fig 3.5. We expect that the feedback between adhesion area and propulsion strength only affects cell motility when the adhesion area is below or near the saturation point s.

New behaviours ranging from slow cells to stick-slip

Here, we will look at parameter combinations which result in adhesion areas below or around the saturation threshold s. We choose $s = 0.1$ and $b = 0.5$, and from the previous simulations we know that p_s is the main parameter controlling adhesion area, so we chose $p_s \leq 0.004$.

We observed different types of behaviour depending on p_s (Fig 3.6, Supplementary Video S2). For very low values of p_s (Fig 3.6A), cells have only a small number of tiny adhesion patches and thus very small adhesive area. Furthermore, they disperse little (Fig 3.6A). Despite their low dispersion, their motion can still be described well with Eq. 3.2 or with Eq. 3.4 with $\alpha = 0.974$, so the type of motion can still be classified as a persistent random walk, albeit with lower persistence time. When $p_s = 0.004$, the mean adhesive area is approaching the saturation point. However, the diffusion and persistence are lower compared to the model without the adhesion-protrusion feedback, but velocity is comparable (Fig 3.6B). In between these

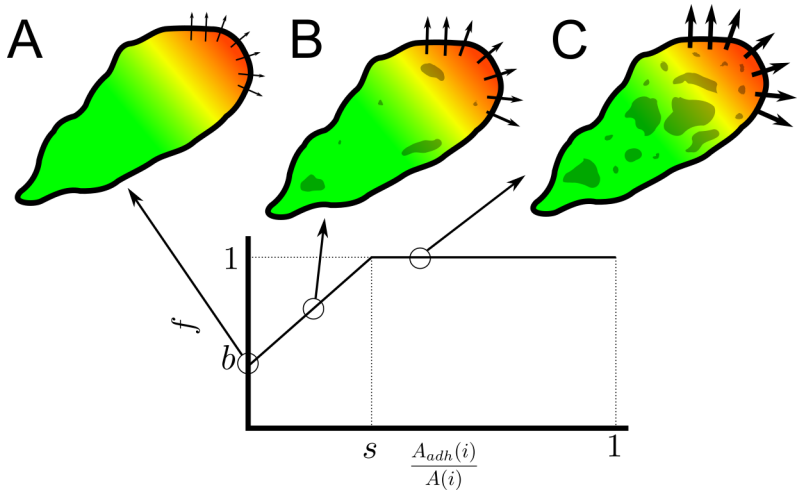

FIGURE 3.5: **Schematic representation of the adhesion propulsion feedback.** Colour schemes are similar to Fig 3.1A. Arrow width corresponds to the effective protrusion strength $f\lambda_{Act}$. A) In the absence of adhesions, the propulsion prefactor f is equal to the base level b. B) Below the saturation point s, f increases linearly with adhesion area. C) Above the adhesion area saturation point s, prefactor f, and thus effective protrusion strength $f\lambda_{Act}$, are maximal.

two adhesive regimes, there is the possibility of stick-slip behaviour (Fig 3.6C), with clear bursts of adhesive area coupled with increased speed.

There is a clear difference between the model with and without feedback of adhesion area onto propulsion strength. For low adhesive areas, we expect the two models to converge to the Act model with an effective propulsion strength equal to the set λ_{Act} for the version without feedback, and an effective propulsion strength of $b\lambda_{Act}$ for the version with feedback. Looking at average velocity and the diffusion constant, this expectation is met (Fig 3.7). Similar to the results in Fig. 3.3, the effect of adhesion energy λ_{adh} is larger on the diffusion of cells than on their velocity for the model both with and without feedback between adhesion and propulsion. Remarkably, there is a slight difference in mean adhesion area between the models. This small effect is likely due to closing the feedback loop between adhesions and propulsion, as *de novo* adhesion formation depends on Act-front presence, which becomes less pronounced when adhesion area is low in the model with feedback.

Our model with feedback shows that cells with low adhesive area have low displacement compared to cells with higher adhesive areas. Overall, by adjusting the parameters p_s and λ_{adh}, the model is able to reproduce

the three behaviours of B cells observed on fibronectin: low attachment with low displacement, dynamic adhesion area with high displacement and sustained attachment with low displacement [143].

3.2.5 Adhesion growth dynamics change persistence time

So far, we have only looked at the effects of new adhesion formation p_s and adhesion strength λ_{adh} on adhesive area and cell motility. However, the adhesive area is also in part determined by the two parameters p_e for adhesion growth and p_d for disbonding adhesions. To gain further insight in the impact of adhesion dynamics on cell motility, we also explored parameter settings resulting in the same adhesion area but with different adhesion cluster size distributions, by varying the formation rates for new adhesions (p_s) and adhesion growth (p_e). Fig. 3.8 shows the results of two such parameter settings resulting in the same average adhesion area. One parameter set obtains its adhesive area mostly through the formation of new adhesions ($p_s > p_e$, Fig. 3.8A: blue), whereas the other more rapidly grows out adhesion clusters ($p_s < p_e$, Fig. 3.8A: orange, see also Supplementary Video S3). This results in different cluster size distribution (Fig. 3.8B), with only small clusters when $p_s > p_e$ (blue line), and small clusters combined with a few large ones when $p_s < p_e$ (orange line). Aside from the different adhesion cluster size distribution, cell motility also differs between the two situations.

First, the velocity distribution has a slightly higher mean for the many-small-cluster (blue) setting, but also appears more bimodal than the few-large-cluster (orange) setting (Fig. 3.8). Analysing the MSD shows more differences: the few-large-cluster (orange) setting shows an earlier start of the final linear regime. The onset of this regime corresponds to the persistence time, which we obtained by fitting the MSD with Eq. 3.2 as well as Eq. 3.4. The fitted persistence times confirm this observation: the few-large-cluster (orange) setting has about 25% lower persistence time than the many-small-cluster (blue) setting. So not only the total adhesion area influences cell motility, but also how that area is distributed over adhesion clusters and where those clusters are located. This further shows that the dynamics of cell-matrix adhesion influence cell motion and can be a key component of cell motion plasticity.

The distribution of the adhesion clusters over the cell is reminiscent of the difference between walking and gliding T cells [144]. The sliding T cells had a large contact area at the cell front, quite similar to the blue setting in Fig. 3.8, which derives its adhesion area mainly from the Act-dependent formation of new adhesions. The walking T cells, in constrast, showed

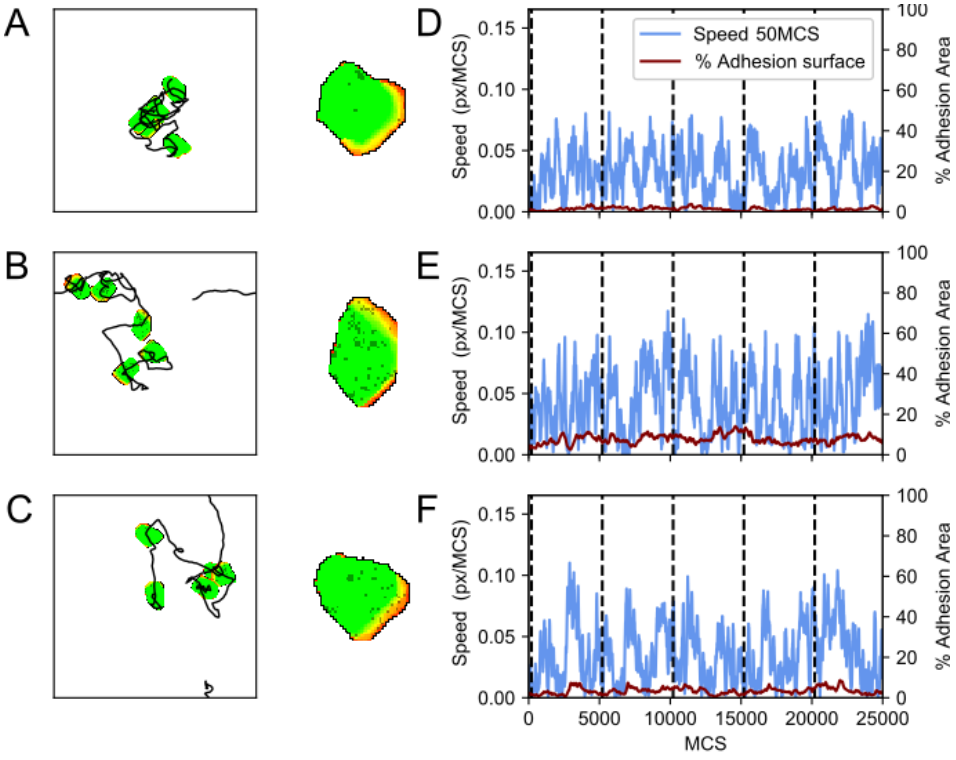

FIGURE 3.6: **Simulations of the model with adhesion-propulsion feedback.** On the left, a display of a single cell at 5000 MCS intervals combined with trajectory of the cell centre. Each trajectory starts in the middle and periodic boundaries are used. In the middle, a close-up of the cell with the adhesion displayed in a darker colour. On the right, a plot of the cell's velocity and percentage of the cell's area containing adhesions corresponding to the track on the left. Parameters are: A) $\lambda_{adh} = 100$, $p_s = 0.001$, B) $\lambda_{adh} = 100$, $p_s = 0.004$, C) $\lambda_{adh} = 100$, $p_s = 0.0025$. Furthermore $p_d = 0.001$ for A, B and C. These simulations are also available as Supplementary Video S2.

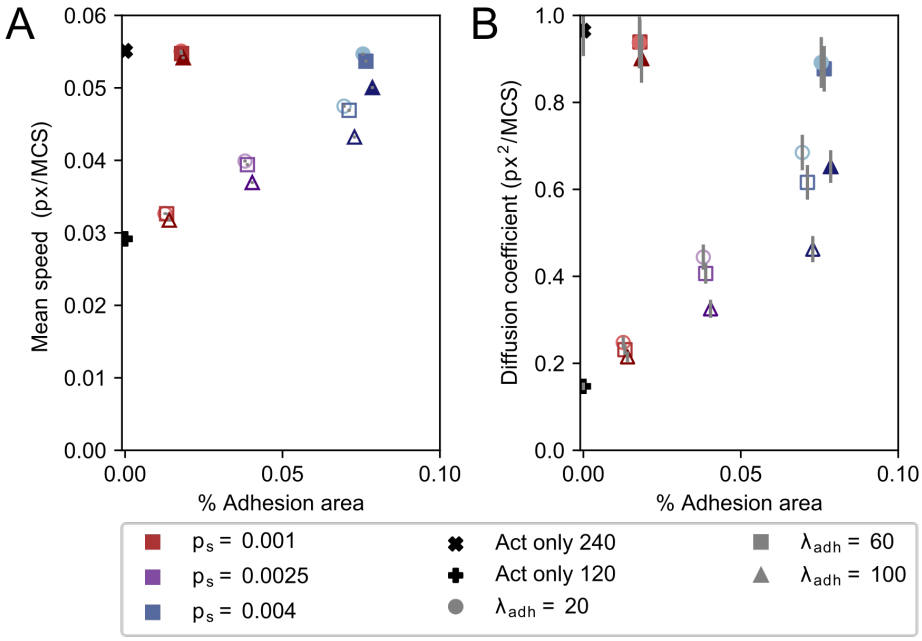

FIGURE 3.7: **Mean velocity, diffusion coefficient and adhesion area differ between the model with and without adhesion-propulsion feedback** Mean velocity (A) and diffusion coefficient (B) plotted against mean percentual adhesion area for different values of parameters p_s and λ_{adh}. Each dot represents the mean over 1000 independent simulations. Filled symbols are results from the model without adhesion-propulsion feedback, and empty symbols show results from the model with adhesion-propulsion feedback. Different colours indicate different p_s, where shades from light to dark and marker symbol indicate $\lambda_{Adh} \in \{20, 60, 100\}$. Error bars indicate 95% confidence intervals.

contact area also at the rear of the cell, and had multiple distinct contact areas. The orange setting from Fig. 3.8, where adhesion area mainly grows by adhesion expansion rather than new adhesions, resembles this adhesion distribution over the cell. However, the mean speed found in [144] is higher for walking cells and lower for gliding cells, opposite to the two parameter settings shown here. Nonetheless, our model suggests that the different processes by which adhesions form, such as *de novo* at the cell front or by extending existing adhesion patches, can underlie the differences between walking and gliding cells.

3.3 Discussion

Here, we have presented an extension of the CPM-Act model with dynamic cell-matrix interactions. In this model, cell-matrix adhesions can develop *de novo* in an Act-dependent manner, and adhesion patches can shrink and grow. Furthermore, adhesions can break for a set energy cost. We first studied the effect of two parameters, namely the energy cost of breaking adhesions λ_{adh}, also interpretable as the strength of an adhesion bond, and the probability with which new adhesions form at the polarized front of the cell. Cells with low adhesion area perform a high speed, highly persistent random walk. The simulated cells slow down for increasing bond strength, but also for increasing *de novo* adhesion formation. For very high bond strengths, the cells can even get stuck. Stuck cells show a different type of motility which is persistent on a short time scale, but subdiffusive on long-time scales. By adding feedback between cell-matrix adhesion area and propulsion strength, a richer behavioural repertoire can be reproduced for low adhesive areas. With this feedback, simulated cells with very low adhesive areas have low dispersion, as their propulsion strength is weakened. Cells with slightly higher adhesive areas can show temporary spurts of increase in adhesion area combined with increase in velocity. Finally, we studied the effect of the processes that form the adhesion area and found that adhesion cluster size distribution can affect cell motility. Cells with many small adhesion clusters at the cell front perform a more persistent motion than cells that have fewer but larger adhesion clusters located at the centre and the back of the cell, even while total adhesion area is equal.

For long-term behaviour in our model, we mostly observed diffusive behaviour or, for more extreme λ_{Act} and p_s values, subdiffusive behaviour. The B cells observed by Rey-Barroso et al. performed long-term diffusive behaviour. Superdiffusive behaviour has also been observed in mammalian

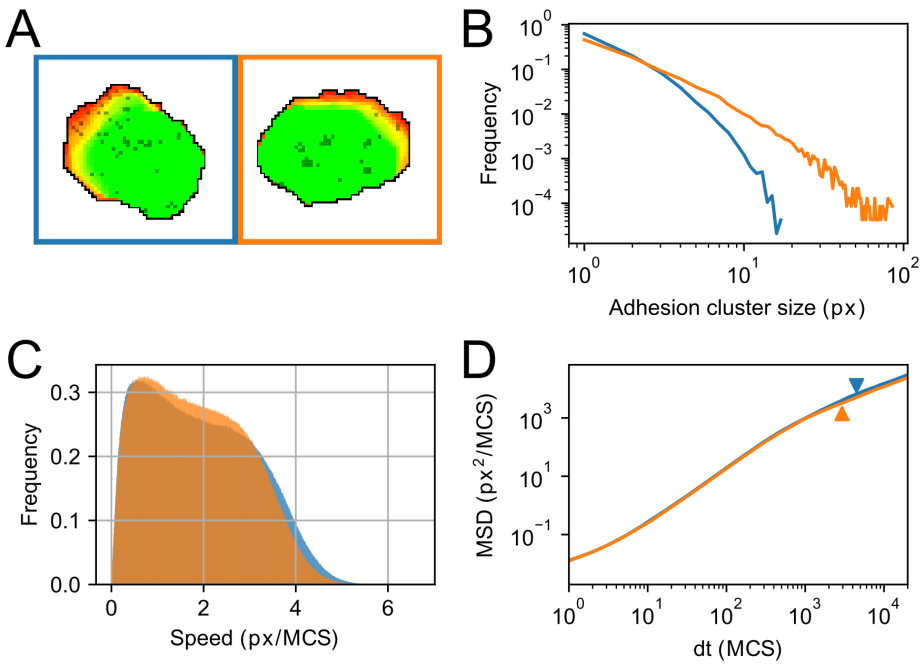

FIGURE 3.8: **Adhesion growth dynamics influence adhesion cluster size, cell speed and MSD** (A) Example of different adhesion cluster size for different parameter values of p_s and p_e. Blue: $p_s = 0.003$, $p_e = 0.0015$ resulting in a multitude of single grid point sized adhesions. Orange: $p_s = 0.001$, $p_e = 0.004$, resulting in a small number of larger clusters. Colours in B,C,D correspond to these parameter settings. (B) Distribution of cluster sizes for 1000 independent simulations for each parameter setting on a logarithmic scale. Distribution of blue does not exceed cluster size 20 (C) Distribution of instantaneous velocity of 1000 independent simulations for each parameter setting. Mean speed for orange is lower compared to blue (D) Log-log plot of MSD. The onset of the second linear regime (log-log slope approximately equal to 1) is marked with an arrowhead in corresponding colours. This regime starts at smaller dt for the orange curve compared to the blue curve, which corresponds to a lowered persistence time compared to blue. Simulations are also available as Supplementary Video S3.

cells. The murine T cells in [56] showed superdiffusive behaviour, but have only been tracked for a relatively short time (∼10 min), so their diffusive behaviour on longer time scales is unknown. The Madin-Darby canine kidney cell in [160] have been tracked for a much longer time (∼1000 min) and perform superdiffusive walks at both short and large time scales, and their velocities show long range correlations in time. What causes these long-time correlations is unclear. As we have not seen our model display long-term superdiffusive behaviour, and because there is no long-term memory in our current model, we think that some molecular memory could play a role in cell superdiffusivity.

Intercellular variability

When comparing the resulting behaviours of this model with the motility patterns described in [143] and [144], we were able to capture the floating, stepping, and pivoting behaviour observed in B cells on fibronectin, by just altering adhesion bond energy cost and *de novo* adhesion formation, as well as the walking and gliding behaviour observed in T cells on ICAM and casein, by adjusting *de novo* adhesion formation and adhesion patch growth. Noteable is that these different types of motility were all observed within the same populations of cells.

Variability among individual isogenic cells has also been described in chemotaxis of *Dictyostelium discoideum* cells [164] and keratocyte shape and motility [39]. Moreover, a single random walk model could not describe the motion of a CD8+ T cell population, but division of the population into Brownian walkers and persistent walkers could describe the motion of the population [165].

Our model can aid in pinpointing what underlies the intercellular diversity. It shows that a small degree of variability in adhesion formation rate, adhesion detachment rate, adhesion distribution, or in the coupling from adhesions to cytoskeleton can lead to distinct migration properties and even modalities. It is therefore tempting to speculate that lymphocyte populations observed *in situ* or in cultures harbour a certain degree of heterogeneity in some of these pivotal parameters. Already, different subsets of differentiated CD4+ T cells (Th1/Th2/Th17 subsets) have been described to harbour distinct motility properties both *in vitro* and *in vivo* [166, 167]. These differences appear to be explained by distinct molecular equipment in terms of adhesion and cytoskeleton dynamics. Interestingly, these differences have been proposed to support distinct search strategies aligning with the fact that these cell subsets target different types of pathogens. Actually, our study provides a mechanistic framework to ask such questions

and address them experimentally (e.g., by measuring integrin expression levels among individual cells by flow cytometry, monitoring size and distribution of adhesions with super-resolution microscopy approaches). For instance, to fully understand the mechanisms underlying the differences between B cell motion on fibronectin versus collagen, more knowledge on this intercellular diversity in integrin dynamics would be beneficial. This knowledge can then be used in further simulations to choose parameters for individual cells from a suitable range and reproduce the fast Brownian motion on fibronectin with more adhesive area as well as the slow persistent motion on collagen IV with lower adhesive area.

How to disentangle velocity and persistence in the model

Although our model provides a plausible explanation for the impact of cell adhesion on subdiffusive cell motility, it does not reproduce the observation that B cells move faster and in a Brownian fashion on fibronectin, but slowly and persistently on collagen IV. This could be due to the fact that in our model, persistence and motility (dispersion) are highly correlated: fast cells also show high persistence, so it is unlikely that simulations will result in slow but persistent motion. An experimental study showed a universal coupling between cell speed and cell persistence (UCSP) to be mediated by actin flow [168], as actin flow stabilizes cell polarity. In our model, the actin flow is modelled phenomenologically by the Act model [73], which displays this UCSP as well [147].

Currently, the Act-extension, and specifically λ_{Act} is the only model component that is influenced by the adhesion dynamics. If adhesions stabilize actin fibres, it is also reasonable to make Max_{Act} or the speed of Act degradation dependent on the presence of adhesions. Otherwise, other aspects of cell locomotion, already captured in our model or not, could be influenced by cell-matrix interactions and lead to slow but persistence motion on collagen IV.

Where the Act-extension mainly models the front of the cell, many locomotion-related processes also involve the rear of the cell. Myosin-II contraction pulls the back of the cell towards the front and can increase cell velocity [144]. Preliminary studies with our model show that cell velocity can be changed by altering the weight of the perimeter constraint, or by changing the contact energy between cell and matrix. Both of these components model myosin-II contractility indirectly. Part of this cortical tension is transferred onto the matrix through adhesions [169, 170]. An interesting question is whether the cortical tension is also influenced by the presence of adhesions. Furthermore, myosin-II is suggested to be a

polarization cue and to be transferred to the back of the cell by retrograde actin flow and could possible also alter persistence of cell polarization [168]. An interesting direction for future research would be to study how the retrograde flow is influenced by cell-matrix adhesions and how this may affect the UCSP.

Matrix rigidity and mechanistic feedback between integrins and matrix

We have modelled cell-matrix adhesions as a simple on/off-switch, with a set amount of energy required to break the adhesion. In reality, the adhesion process is much more complex, involving mechanistic feedback between integrins and the matrix. Hence, both matrix rigidity and the cell's ability to generate force influence cell shape and cell motion. When it comes to modelling this feedback, different approaches have been used already. In Copos et al. [145], adhesions were modelled as mechanosensitive bonds. In Ziebert et al. [65], adhesions ruptured when they exceeded a maximum length. In Shao et al. [66] the probability of adhesion rupture increased with force. In Löber et al. [67], the matrix deformation was also taken into account, leading to non-trivial motion such as bipedal motion.

Modelling matrix deformation or displacement of adhesion sites within the CPM is challenging, but a lot of progress has been made recently. Methods to estimate forces within the CPM cell have been developed, either based on cell shape or on the Hamiltonian [171, 62]. The CPM has also been combined with a finite element method to model matrix traction forces with feedback between the CPM and FEM [171, 172]. Moreover, cell-matrix adhesions were recently introduced into this framework [173] as focal adhesions with force dependent growth, and smaller focal adhesions being easier to dislodge from the ECM. In the observed B cells, however, adhesions are not structured into focal adhesions. Nonetheless, these novel methods can be used to improve the realism of our model, both on the side of cell-matrix bonds, as well as the side of matrix deformation and matrix stiffness.

Adhesion patch detachment

In our current model, adhesion patch detachment occurs through a stochastic process of loss of sites combined with the energy requiring retraction. This part of the model can be refined in several ways. First, it is known that myosin-IIA, besides rear-end retraction, is also involved in the detachment of adhesion patches in T cells [144, 174]. Myosin-II increases the forces

exerted on the adhesions. Combining mechanistic feedback between adhesions and the matrix, as proposed in the previous paragraph, with an explicit model of myosin-II near adhesion patches could result in more realistic patch dynamics. Second, detachment at the rear of the cell is also regulated by other molecular processes. Talin and moesin, both scaffolding proteins between integrin and the cytoskeleton, can compete with each other, but have different properties. While talin connects the cytoskeleton to integrins, moesin inactivates integrin, thereby decoupling the adhesion from the cytoskeleton [175]. This process mainly occurs at the rear of the cell. Integrating the activities of talin and moesin into our model can refine the de-adhesion process at the cell rear currently modelled by an energy threshold.

Conclusion

In conclusion, we have introduced a CPM model combining the Act model [73] with dynamic cell-matrix adhesions. We have shown that our model is capable of extending the repertoire of motility types within the CPM, both from a detailed cellular level, as well as on a statistical level (Figure 3.9). Besides the persistent random walk that emerges from the Act model, our model is also able to reproduce a short-term persistent but long-term subdiffusive random walk. While adhesion dynamics are simplified, our model can show the different types of motion observed in individual B cells on a fibronectin substrate, such as reduced motility for non-attached cells, a walking motion, and pivoting due to sustained attachment, as well as the walking and gliding motion of T cells on ICAM or casein substrate. Here we uniquely link short-term molecular scale to the long-term cell behaviour scale to learn about those molecular parameters that explain the plasticity of immune cell motility upon interaction with varying substrates. In particular, our study highlights that the interplay between adhesion formation, adhesion expansion and adhesion strength determine the turn-over of the adhesion area which regulates cell speed and persistence. Furthermore, the model provides a mechanistic framework for generating experimentally testable hypotheses.

3.4 Methods

In this work, we model the different cell motilities of cells adhering on flat matrix surfaces. The basis of our model is the Cellular Potts model.

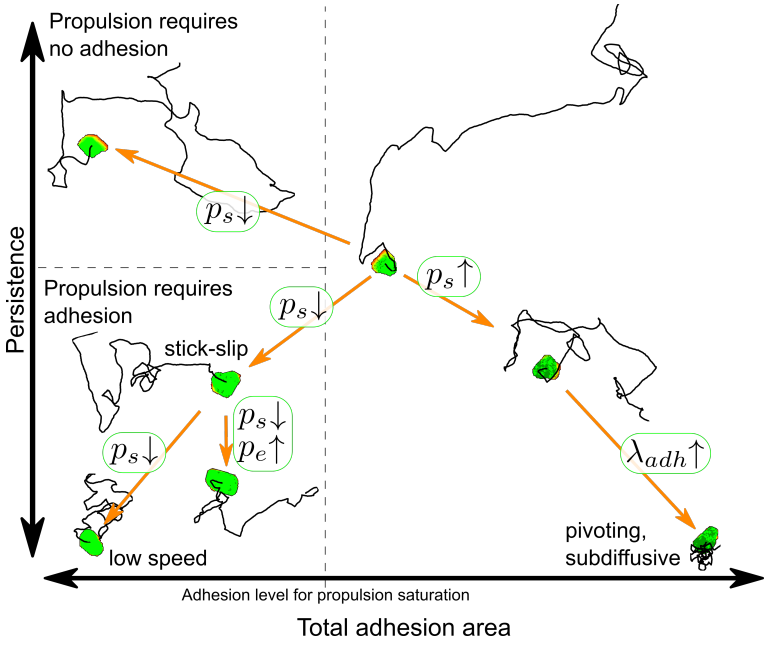

FIGURE 3.9: **Overview of the motility modes possible in the model and which parameters govern the transitions between them.** For each motility mode, a representative cell and its trajectory are plotted in a persistence versus total adhesion area plane.

3.4.1 Cellular Potts model

The Cellular Potts model (CPM) is a grid-based model. Grid points are assigned an identity σ, indicating to which cell they belong. All grid points with the same σ together form a single cell. The model evolves through time by doing copy attempts: two neighbouring grid points are selected and the σ of one grid point is trying to be copied into the other grid point. Whether this copy attempt actually occurs is decided by the Hamiltonian $\mathcal{H}$, which describes the energy of the system. Different Hamiltonians have been proposed for different CPM models. We use the following:

$$\mathcal{H} = \sum_{u,v \in \text{Neighb.}} J_{\tau(\sigma_u),\tau(\sigma_v)}(1 - \delta_{\sigma_u,\sigma_v}) + \lambda_A \sum_{\sigma}(a_\sigma - A_\sigma)^2 + \lambda_P \sum_{\sigma}(p_\sigma - P_\sigma)^2$$

The first term describes the contact energies between cell and medium or between two cells. The second term describes an area constraint, with A_σ being the target area of cell σ and the third term describes in similar ways a perimeter constraint with P_σ the target perimeter of cell σ.

A copy attempt is accepted depending on the change in Hamiltonian $\Delta\mathcal{H}$ it causes:

$$P(\Delta\mathcal{H}_{\mathbf{x}\to\mathbf{y}}) = \begin{cases} 1 & \text{if } \Delta\mathcal{H} < 0 \\ e^{-(\Delta\mathcal{H}/T)} & \text{if } \Delta\mathcal{H} \geq 0 \end{cases}$$

Here, T plays the role of an effective temperature and controls the amount of variability we allow to happen. Higher T will allow more thermodynamically unfavourable copy attempts to succeed.

A measure of time in the CPM is the Monte Carlo Step (MCS). Within one MCS, the expectation is that each grid point has been updated once. We use a rejection-free algorithm that only considers attempts between neighbours of different σ to speed up simulations [69, 176].

3.4.2 Cell motility

Cells move by making protrusions through actin polymerization and form cell extrusions like filopodia, pseudopodia and lamellipodia. Actin polymerization in the CPM has previously been modelled in a phenomenological way by Niculescu et al. [73]. We also use this extension to model the actin polymerization. This extension adds an extra layer to the CPM, described as the Act-layer. The values of this layer vary between 0 and a maximum value Max_{Act}. Grid points that are newly added to a cell obtain Act-value Max_{Act} and each MCS the values of the Act layer are lowered

by 1 until 0. The Act-extension is added to the CPM as an extra term for the change in Hamiltonian $\Delta\mathcal{H}$, namely as $\Delta\mathcal{H}_{Act}$. For $\Delta\mathcal{H}_{Act}$, the local geometric mean of Act-values of both the expanding and retracting grid points are calculated and compared. Then, $\Delta\mathcal{H}_{Act}$ favours the grid point with the highest mean in the following way:

$$\Delta\mathcal{H}_{Act}(u \to v) = \frac{\lambda_{Act}}{\mathrm{Max}_{Act}} \left(\left(\prod_{y \in V(u)} Act(y) \right)^{1/|V(u)|} - \left(\prod_{y \in V(v)} Act(y) \right)^{1/|V(v)|} \right)$$

with $V(x)$ describing the neighbourhood of grid point x in the same cell. Here λ_{Act} is the weight given to this model component.

Adhesion to the matrix makes actin polymerization more efficient in protruding the cell membrane [161, 162, 163], by transmitting the force to the matrix. We add feedback between the cell adhesions and the actin polymerization, by strengthening the force produced by polymerization upon increase in adhesion area. This is done by multiplying λ_{Act} with factor f defined as follows:

$$f = \begin{cases} b + \frac{1-b}{s} \frac{A_{adh}(i)}{A(i)} & \text{if } \frac{A_{adh}(i)}{A(i)} \leq s \\ 1 & \text{if } \frac{A_{adh}(i)}{A(i)} > s, \end{cases}'$$

Here $A(i)$ denotes the area of cell i, and $A_{adh}(i)$ denotes the adhesive area of the cell i, b the value of f when there are no adhesions, and s the value at which f saturates.

3.4.3 Adhesions to the substrate

The adhesions of a cell to the extracellular matrix are modelled as a third layer in the CPM. A grid point x in this layer can have either $Adh(x) = 0$, no adhesion, or $Adh(x) = 1$, when it denotes an adhesion patch of the cell. Adhesion dynamics are governed by four processes: spontaneous formation of new adhesions, adhesion patch expansion, adhesion patch retraction, and rupture of adhesion through retraction of a cell. We describe each of these processes below.

New adhesion sites

New adhesions form when the cell membrane comes in close enough contact with the extracellular matrix such that integrins can bind to the matrix. This process is dependent on actin polymerization, membrane

protrusion and polarized distribution of integrins [151, 152, 153]. We model *de novo* adhesion formation through a stochastic process. Each MCS a grid site within a cell can turn from non-adhesion to an adhesion site. This can only happen when the local geometric mean of the Act layer exceeds the value $0.75\,\mathrm{Max}_{Act}$, i.e. when:

$$\left(\prod_{y\in NB(x)} Act(y)\right)^{\frac{1}{|NB(x)|}} \geq 0.75\,\mathrm{Max}_{Act}$$

Then, the probability for a cell to form a new adhesion at that grid site is given by the probability parameter p_s.

Adhesion patch expansion

Once adhesion patches are formed, they can increase in size. Multiple processes underlie this expansion. First, once the cell membrane is attached to the matrix, it fluctuates less, allowing for easier attachment of new integrins [154]. Secondly, the curvature of the cell membrane influences the intermolecular forces, favouring aggregation of integrins [155, 156].

We do not model integrin recruitment and membrane curvature, but choose to model adhesion patch growth phenomenologically. Jacobelli et al. [144] observed that adhesion patches grow radially, with some bias in the direction of the cell front. Hence, we model adhesion patch expansion as an Eden-like growth model [157], known to give roughly circular shapes. While updating the adhesion layer, once a grid point containing an adhesion is selected to be updated, we also select a random neighbour. If that neighbouring grid point contains no adhesion, it can form an adhesion with probability p_e.

Adhesion patch retraction

Aside from patch expansion, patch retraction can also occur. Patches will partially dissolve spontaneously, as they are out-of-equilibrium systems [177]. Also, Myosin-II contraction is involved in patch retraction [144], which occurs concentrically. Following these observations, an adhesion site x in this model can spontaneously decay with a probability depending on the adhesion status of its neighbours.

$$P(x \text{ will de-adhere}) = p_d \cdot \left(\frac{|\{nb \in NB(x) | Adh(nb) = 0\}|}{|\{nb \in NB(x)\}|}\right)^2$$

with $NB(x)$ the neighbourhood of x. Thus, the higher the number of non-adherent neighbours, the higher the probability that the site loses its adhesion.

Adhesion rupture through retraction

Adhesions can also disbond by force. It is know that integrin shows catch-slip bond behaviour [178, 179]. Since we do not directly model forces in the CPM, and since we do not model matrix stresses, we simplify the rupture of an adhesion to a constant amount of energy required to break an adhesion upon cell retraction. This energy is added to the change in Hamiltonian the following way:

$$\Delta\mathcal{H}_{adh}(u \to v) = \lambda_{adh} Adh(v)$$

Here $\sigma(u) \neq \sigma(v)$ and the cell $\sigma(v)$ is retracting.

3.4.4 Order of layer updates

This model has three layers: one for the grid site identities σ, one for the Act-values and one for the adhesions. These three layers are updated in the order σ - adhesions - Act-values. The σ-layer is updated through the rejection free Metropolis algorithm. During the σ-update, Act-values and adhesion updates regarding the relocation of the cell are executed immediately: e.g., for copy attempts that let a cell retract from a grid point, we do directly update the Act-values and adhesions of that site. After the σ-update, we update the adhesion layer asynchronously: we iterate, in random order, over the grid points within the cell and execute the processes described in the Adhesions subsection. Lastly, we update the Act-layer: every Act-value is diminished by 1 until 0. These three updates together constitute one MCS and this cycle is repeated for a set number of MCS.

3.4.5 Simulation parameters

During our different simulations, many parameter values were kept constant (Table 3.3). All simulations were done on a 300×300 pixel grid with periodic boundaries with a single cell. Parameter values that were not constant are shown in Table 3.1. For the simulations in Fig 3.2, 3.3 and 3.4, $p_d = 0.0064$, and p_s and λ_{adh} varied according to the figure legends. For simulations shown in Fig 3.6 and 3.7, $p_d = 0.008$ and again λ_{adh} varied according to the figure legends. The Act-only simulations in Fig 3.3 and Fig 3.7 were run with all adhesion dynamics parameters equal to zero: i.e.,

TABLE 3.3: List of parameter values kept constant during all simulations. Values are arbitrary units, unless specified otherwise.

Parameter	Description	Value
T	temperature	30
A	target area	1000 px^2
λ_A	weight area constraint	50
P	target perimeter	350 px
λ_P	weight perimeter constraint	4
λ_{Act}	weight of Act model	240
Max_{Act}	Act lifetime	120 MCS
$J_{medium,medium}$	adhesion energy between medium	0
$J_{cell,medium}$	adhesion energy between cell and medium	35
Total MCS	simulation duration	25000 MCS

λ_{adh}, p_s, p_e, and p_d were all zero. For all simulations, $\lambda_{Act} = 240$, except for the specific Act-only simulations in Fig 3.7 with $\lambda_{Act} = 120$. For the simulations in Fig 3.8, p_e and p_s were varied, see figure legend. The parameters not mentioned in the figure legend are $p_d = 0.0004$, $\lambda_{adh} = 60$, $b = 0.5$, $s = 0.12$.

Acknowledgments

G.T. gratefully acknowledges the Indian Institute of Science to serve as Infosys visiting professor at the Centre for Ecological Sciences in Bengaluru. L.v.S. would like to thank the French Embassy in the Netherlands for the Bourse d'Excellence Descartes de stage. We also thank SURFsara for the support and computing time in using the Lisa cluster computer.

3.5 Supporting information

The supplementary videos can be accessed online at `https://doi.org/10.1101/2021.06.09.447692`.

S1 Video Cell velocity and persistence drop with increasing values for adhesion formation and adhesion strength.

S2 Video Cell velocity and persistence drop in the model with feedback from adhesions onto cell protrusion when adhesive areas are small.

S3 Video Similar adhesive area sizes lead to different motility when adhesion growth is dominated by the actin-dependent formation of new adhesions versus the growth of existing patches.